DECAY RATE CHANGES IN RADIOACTIVE GAMMA EMISSION AS AFFECTED BY 18 MeV PROTON CYCLOTRON

by

Jonathan WALG [1]***, Jon FELDMAN*** [2]***, and Itzhak ORION***[1*]

[1] Department of Nuclear Engineering, Ben-Gurion University of the Negev, Beer-Sheva, Israel
[2] Sharett Institute of Oncology, Hadassah University Hospital, Jerusalem, Israel

Scientific paper
https://doi.org/10.2298/NTRP2401001W

Previous efforts to investigate changes in the decay constants of radioactive nuclides discovered that solar flares can temporarily alter radioactive decay rates. Thus, discerning whether external factors affect radioactive decay rates is vital for understanding nuclear processes. This study sought to explore the effect of neutrinos on radioactive nuclei by constructing a gamma radiation detection system that employs a radioactive source in front of a neutrino emission system. Responding to cyclotron operations, each of the four detection systems registered gamma count rate decreases. The results of this study confirm that rises in neutrino flux affected the decay rates of the examined radioactive nuclides. Here we provide significant evidence that neutrinos affect the radioactive decay process. Neutrino detection is challenging due to the minuscule absorption in a stable nucleus. However, the study found a greater probability of radionuclides interaction with the neutrino.

Key words: cyclotron, radioactivity, neutrino, gamma radiation

INTRODUCTION

Several studies have demonstrated that solar flares modify the radioactive decay constant. The change in the radioactive decay constant due to solar flares motivated us to seek the origins of this effect.

Researchers first observed anomalies in the decay of ^{54}Mn in 2006 [1]. The resulting measurements demonstrated changes in the count rate of the gamma rays associated with the radionuclide decay, which undergoes a radioactive electron capture process by the nucleus. Such results of the decay constant changes were counter-speculated by Pomme [2-5] but are not relevant to this study. The current study focuses on a controlled neutrino source, while Pommé's arguments concern constant decay oscillations. Furthermore, this study is performed with an artificial production of neutrinos and does not focus on solar or cosmic events's influence. Therefore, Pomme's claim does not apply here. In radioactive decay, a stochastic process in an unstable nucleus determines a constant probability of particle emission. Every radioisotope emits particles in a unique process, with a specific decay constant expressed in units of disintegrations per second. The nucleus emits energy and releases nuclear radiation, meaning the release of gamma-ray radiation, a beta-minus particle (electron), a beta-plus (positron), a neutron, an alpha particle, or a neutrino or an anti-neutrino. In certain cases of nuclear decay, the nucleus emits more than one particle at the same time, or in a chain of disintegration. The decay constant is considered a physical constant, according to measurements taken over the period during which the various radioisotopes decay [6]. The radioactive decay constant for a variety of isotopes ranges from 10^6 s^{-1} to 10^{-10} per year. The specific activity of the radionuclide is determined by multiplying the decay constant by Avogadro's constant divided by the molar mass.

Certain studies have investigated whether the decay constant remains the same under all conditions [7]. Jenkins' results concerning count rates of gamma radiation demonstrated a decrease over three different periods, with the changes occurring not as a result of statistical fluctuations but rather due to, among other factors, powerful solar flares (class X-M) [1]. Following this publication, scholars suggested that changes in the radioactive decay constant of ^{54}Mn result from a rise in the neutrino flux originating from the sun during solar flares. They discerned a correlation between the occurrence of a solar flare and changes in the decay rate of ^{54}Mn. The nuclear activity that takes place in the sun is measured constantly by GOES series satellites, revealing power changes in the X-rays that reach an orbital path around the Earth. A solar flare is charac-

* Corresponding author, e-mail: iorion@bgn.ac.il

terized by a rise in the intensity of the flux of elementary particles, including the neutrino.

The physicist W. E. Pauli hypothesized that the neutrino could offer a solution to the problem of balance of momentum and energy in beta decay. The neutrino, an elementary particle lacking charge, is emitted together with the electron from the nucleus in a process influenced by the weak nuclear force field [8]. This particle, a fermion with a 1/2 spin and minimal mass (less than 0.2 eV), was presumed to be massless [9], however, recent studies on different fronts have sought to establish its mass [10, 11]. As early as 1958, Raymond Davis measured a neutrino using an inverted beta process in which the neutrino was captured by a stable ^{37}Cl nucleus close to a nuclear reactor that served as the source of anti-neutrinos [12], and in 1970, Davis established a detector using a tank of stable chlorine solution to measure the neutrinos originating from the sun [13, 14].

The most recent estimations regarding solar neutrino flux are based on the total luminosity of the sun [15]. The estimated neutrino flux is distributed *vs*. the neutrino energy, hence, the estimated flux strongly varies depending on the nuclear reaction that occurs. The proton-proton (pp) reaction in the sun emits low-energy neutrinos with flux ~10^{10} cm^{-2} s^{-1}, and the carbon-nitrogen-oxygen (CNO) reaction emits flux ~10^{8} cm^{-2} s^{-1}, resulting in higher energy neutrinos [16]. However, the experimental neutrino flux measurement is in the order of flux ~10^{6} cm^{-2} s^{-1} [14], and the CNO reaction emits flux ~10^{4} cm^{-2} s^{-1}.

Recently, scholars have conducted further intensive studies regarding neutrino measurements using different detectors [17-23], and it is expected that studies will achieve flux values with greater confidence.

Our previous measurements examined the gamma-ray count rate stability of several radioactive sources over a certain period [24, 25]. We constructed a measurement system consisting of a detector shielded by 5 cm thick lead that isolated the detector from background radiation. The laboratory temperature was controlled to ensure that count rate changes did not result from environmental conditions. In October 2018, several solar flares took place. During these solar flares, we measured the count rate of gamma rays from a radioactive source, ^{241}Am. Three decreases in the readings were measured at first, and we found that these fit with the occurrence of the solar flares [24]. In the following months, further solar flares occurred, resulting in decreases that our counting system registered. Following these results in the measurement of gamma-ray emission from an ^{241}Am source, we established further systems to measure gamma radiation from an ^{222}Rn source [26], as well as ^{54}Mn and ^{57}Co sources [25]. Several solar flares took place, and in accordance we detected decreases in the count rates of gamma radiation of ^{222}Rn, ^{54}Mn, and ^{57}Co sources. The effect of solar flares on the count rate of thorium beta radiation was observed utilizing a plastic scintillator as well [27]. Based on the isolation of the system, the only remaining possible explanation for these decreases is a neutrino penetrating the system. Considering these measurements, we suggest that the source of the decrease in count rate is the rise in neutrino flux during solar flares.

To examine this hypothesis, we decided to test a source that is liable to emit neutrinos in a controlled manner, similar to Davis' method [28, 29]. We chose to place the gamma rays measurement system in front of an 18 MeV medical proton cyclotron.

MATERIALS AND METHODS

Gamma radiation measurements

Two main methods are used to detect gamma radiation: crystal scintillation that emits light in response to the radiation, and a solid-state diode that produces electron-holes when exposed to radiation. Currently, most detectors are available with mounted electronics, analyzer hardware, and operating software.

The gamma radiation flux or intensity is attenuated in media due to the medium-specific density and thickness, depending on the photon's energy, as follows

$$I_x \quad I_0 e^{\frac{\mu}{\rho}\rho x} \tag{1}$$

where x is the thickness, ρ – the density, and μ/ρ – the mass attenuation coefficient (depending on photon energy).

The attenuation coefficient is affected by photon absorption or scattering. The eq. (1) is limited to one dimension, while in reality, the attenuation process occurs in 3-D geometry. Also, as in any other type of radiation, the flux decreases due to the law of the inverse square distance.

In matter, any photon absorption ends with a rise in the atomic electron's kinetic energy. The photoelectric effect in the atom is responsible for photon absorption with atomic electron release (ionization). Compton scattering is another process via which photons interact with electrons (free or bonded). A portion of the initial energy is transferred to the scattered electron, and an outgoing photon moves in a different direction. Pair-production is a process whereby there is a probability that photons at above twice the electron-rest-mass energy produce pairs of electron-positron, which will carry kinetic energy. The occurrence of pair-production terminates the photon travel. Photon elastic scattering (Rayleigh scattering) by atoms is unlikely to occur in gamma radiation and diminishes as photon energy increases.

Photons can be produced as secondary radiation in several cases: atomic level X-ray emission, charge-parti-

cles bremsstrahlung, synchrotron radiation, and Cherenkov radiation. Photons may be produced in the detector's surroundings, and therefore they can also be detected.

Scintillators

Scintillators are mostly solid or liquid, making them much more efficient in detecting gamma radiation than ionization gas detectors. Scintillators can be used for spectrometry. The scintillation process consists of light output from electron energy deposition in matter. The scintillator is transparent in light, and therefore a light sensor, such as a photocathode, collects the light to produce and transfer a current pulse throughout a photomultiplier.

The available scintillation materials are not ideal. The ideal scintillation properties for radiation detection are efficient charge particle kinetic energy conversion to light, the light output should be proportional to the deposited energy, short luminescence decay time to produce fast pulses, high optical quality enabling the usage of large detectors, transparency to the emitted light, and an index of refraction similar to glass to allow coupling to a sensor [30, 31].

The light output of a scintillator directly depends on the efficiency related to the energy conversion from radiation into light photons. A fraction of the emitted light can be lost due to imperfections in the crystal's transparency and due to refraction. The fraction of the light passing through in good scintillators varies from 1/20 to 1/40. The overall efficiency is the average ionizing particle energy loss for each photoelectron ejecting the cathode of the photomultiplier. In the photomultiplier, the amount of light translates linearly to charge. The number of electrons emitted from the photocathode is linearly dependent on gamma-ray energy, absorbed energy fraction in the scintillator, efficiency of transfer energy to light, transparency to light, cathode field of view, and sensitivity to light wavelength. A fraction of electrons is collected by the dynodes in the photomultiplier. The outcome charge signal height depends on the number of electrons and the photomultiplier multiplication.

In general, photomultiplier tubes are devices that have a window in which a photocathode is mounted. Behind the photocathode is a collection optics area that leads electrons toward a series of dynodes to multiply the current pulse, ending at the anode. The tube is in a vacuum, and it is protected from magnetic fields. The range of photomultiplier types and materials is extremely vast, depending on the desired response. The overall schematic diagram of the electronic connection to the detector is presented in fig. 1.

Proton cyclotron

To conduct a controlled examination of the effects of neutrinos on radioactive materials, a neutrino is produced using a cyclotron (proton accelerator).

A basic cyclotron contains a uniform magnetic field perpendicular to a vacuumed lattice in the shape of a disk divided into two equal sections (shaped as the letter *D*). The magnetic field causes the charged particles to move in a circular motion as a result of the Lorentz force. The acceleration is induced by a synchronized electric field in the gap between the two half-circle sections when the particle passes through the gap. The particle's radius of rotation increases as a result of the acceleration, hence making the particle trajectory spiral in shape [32]. Cyclotrons for proton acceleration were developed over the course of decades for use in nuclear research, and the proton's final kinetic energy was gradually raised [33, 34]. The basic structure of cyclotrons has also evolved [35]. A medical application of the proton cyclotron was developed for the production of radioactive agents to be used for imaging, such as the production of radioactive fluorine (^{18}F) for use in positron emission tomography (PET CT).

The cyclotron can be fitted with up to 8 targets for producing the most common PET radioisotopes.

$$^{18}_{8}O \quad p \quad ^{18}_{9}F \quad n \tag{2}$$

$$^{18}_{9}F \quad ^{18}_{8}O \quad \beta \quad \nu_e \tag{3}$$

The IBA cyclotrons are operated with a current of protons that can reach up to 300 μA for protons at 18 MeV. The measurement setup is illustrated in fig. 2.

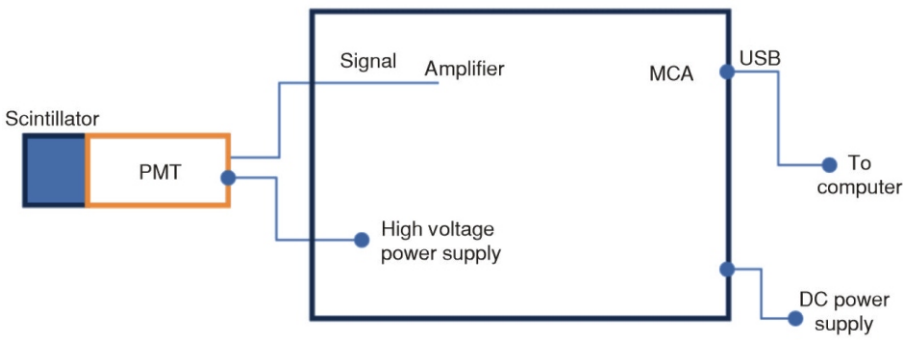

Figure 1. Schematic diagram of a scintillator for gamma radiation spectrometry; the electronic devices are tiny and can be mounted on the PMT end

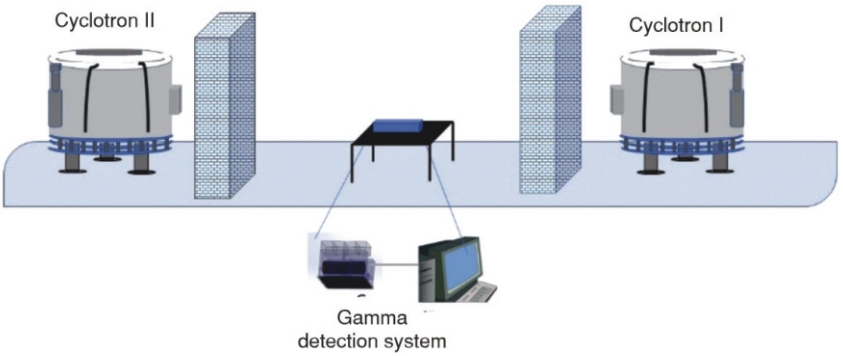

Figure 2. Schematic illustration of a radiation detection system with cyclotrons (dimensions not to scale)

Neutron emission from the cyclotron

Protons hit the target and subsequently, neutrons are emitted. We closely positioned a KCl powder-based detector by the cyclotron walls. In the KCl, a fast neutron interacts with chlorine and emits gamma radiation into a NaI(Tl) scintillator [36, 37].

We performed two measurements in separate positions, one by the ^{222}Rn system and the other by the KCl detector system. The KCl system immediately responded to outgoing neutrons during the cyclotron operation, as shown in fig. 3, in the lower graph. The upper graph in fig. 3 presents the ^{222}Rn count rate data *vs*. time. Figure 3 demonstrates that the ^{222}Rn decrease began around nine hours after the neutron emission. The whole decrease took about six hours due to a long cyclotron operation interval. A comparison of the two graphs indicates that cyclotron operation affected the ^{222}Rn count rate.

Activation

In a medical cyclotron, radionuclides are produced in the target and in surrounding structural materials. The radionuclides produced undergo beta(+) emission or electron capture (EC) process. Therefore, in both cases, a neutrino is emitted along with the process. Table 1 presents the theoretical production of these radionuclides with their yields per cyclotron current per hour, and $T_{1/2}$, from refs. [38-41].

Two cyclotrons were operated at the same time: Cyclotron-I at a distance of 25 m from the measurement system with 5.94 GBq (μAh^{-1}), and Cyclotron-II at a distance of 40 m from the measurement system with 6.21 GBq (μAh^{-1}), as illustrated in fig. 2. Cyclotron-I operated with currents up to 60 μA, and Cyclotron-II operated with currents around 75 μA, and dual cyclotron operations of two hours on average led to decreases.

Cyclotron-I:

Protons flux at activation port $_{p}$

$$_{p} \quad 5.94\,\frac{\text{CBq}}{\text{Ah}}\,2\text{h}\;\;60\;\;\text{A}\;\;\;713\,\text{GBq}\;\;\;7.13\;10^{11}\,\text{s}^{\;1} \tag{4}$$

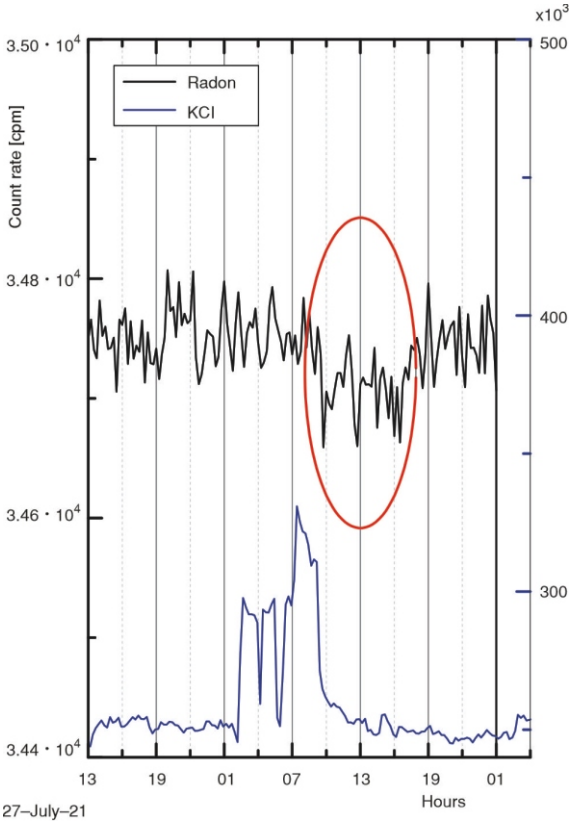

Figure 3. The KCl detector system count rate response to fast neutrons from the cyclotron (line below); and the decrease in ^{222}Rn count rates following the cyclotron operation

Table 1. Theoretical radionuclide production in medical cyclotron based on previous studies [38-41]

Radionuclide	$T_{1/2}$	E_{max} [keV]	Thick target yield [MBq(μAh^{-1})]
^{18}F	109.6 min	635	2960
^{63}Zn [39]	38.3 min	2344	2470 [40]
^{65}Zn	245 d	330	0.2 [41]
^{11}C	20.4 min	960	3820
^{13}N	10 min	1190	4440
^{15}O	122 s	1720	2220

Distance dilution d

$$d \quad \frac{1}{r^2} \quad 1.6\;10^{\;7}\,\text{cm}^{\;2} \tag{5}$$

The ^{18}F production (P_{18F}): 223 GBq (measured)

Neutrino from ^{18}F $\upsilon_{^{18}F}$

$$\upsilon_{^{18}F} \quad P_{^{18}F} \quad d \quad 2.23\ 10^{11}\,s^{-1} \quad 1.6\ 10^{-7}\,cm^{-2} \quad 3.56\ 10^{4}\,cm^{-2}s^{-1} \tag{6}$$

Neutrino from ^{13}N production $\nu_{^{13}N}$

$$\nu_{^{13}N} \sim 5.4 \quad cm^{-2}s^{-1} \tag{7}$$

Led to neutrino from CNO cycle with ν_{CNO}

$$\nu_{CNO} \sim 3 \quad \nu_{N} \quad cm^{-2}s^{-} =$$

$$= 1.6 \quad 10^{5}\ cm^{-2}s^{-} \tag{8}$$

Neutrino at measurement point ν

$$\nu \quad \nu_{^{18}F} \quad \upsilon_{CNO} \quad 2 \quad 10^{5}\ cm^{-2}s^{-} \tag{9}$$

Cyclotron-II:
Protons flux at activation port $_{p}$

$$_{p} \quad 6.21\frac{GBq}{Ah}\ 2h\ \ 75 \quad A =$$

$$= 931\ GBq = 9.31\ 10^{11}\ s^{-1} \tag{10}$$

Distance dilution d

$$d \quad \frac{1}{r^2} \quad 6.25\ 10^{-8}\,cm^{-2} \tag{11}$$

The ^{18}F production ($P_{^{18}F}$): 230 GBq (measured)
Neutrino from ^{18}F $\nu_{^{18}F}$

$$\nu_{^{18}F} \quad P_{^{18}F} \quad d \quad 1.44\ 10^{4}\,cm^{-2}s^{-1} \tag{12}$$

Neutrino from ^{13}N production $\nu_{^{13}N}$

$$\nu_{^{13}N} \sim 2.2 \quad cm^{-2}s^{-1} \tag{13}$$

led to neutrino from CNO cycle with ν_{CNO}

$$\nu_{CNO} \sim 3 \quad \nu_{N} \quad cm^{-2}s^{-1} \tag{14}$$

Neutrino at measurement point

$$\nu = \nu_{^{18}F} + \nu_{CNO} \sim 8 \quad 10 \quad cm^{-2}s^{-1} \tag{15}$$

Total neutrino at measurement point (total)

$$(total)_{\nu} \quad (cyclotron\_\ I)_{\nu} \quad (cyclotron\_\ II)_{\nu}$$

$$\sim 2.8\ 10^{5}\ cm^{-2}s^{-1} \tag{16}$$

During the 15-minute measurement, the system was penetrated by total neutrinos (ν_{total})

$$\nu_{total} \quad (total)_{\nu} \quad t \quad A \quad 2.8\ 10^{5}\,cm^{-2}s^{-1}$$

$$15\ min\ \ 60\ \frac{s}{min} \quad 1(cm^{2}) \tag{17}$$

$$\nu_{total} \sim 2.5\ 10^{8}$$

Even more, flux can be produced by other low-abundance structural materials, such as Zn.

The total neutrino at the measurement point is in a similar order of magnitude to typical solar neutrino flux.

RESULTS

Four measurement systems using ^{241}Am, ^{222}Rn, Thorium, and ^{57}Co tracked alterations in the count rate resulting from changes in neutrino flux emitted by two cyclotrons. Each measurement system consists of a 5.08 cm diameter and 5.08 cm length NaI(Tl) detector facing a radioactive source that tracks total counts at defined time intervals. The NaI(Tl) detector was operated in a total counting mode above 40 keV. The background gamma counts were ~130 cpm (counts per minute).

Neutrino flux is emitted from the two cyclotrons, which are located at around 20 m and around 40 m from the measurement system, as shown in fig. 2. The results were obtained following the operation of two cyclotrons.

The ^{241}Am system

The ^{241}Am source, with activity of around 37 kBq, yielded the following system measurement results.

After nine dual operations of the two cyclotrons, the ^{241}Am system showed nine separate count rate decreases. The counts were collected at intervals of 60 minutes by the detector. Table 3 in the Supplementary information summarizes the results for all nine decreases in the count rate (dips) of ^{241}Am counts. Figure 4 provides an example of a sharp dip in ^{241}Am counts due to the neutrinos emitted by the cyclotrons.

To verify signal detectability and the reliability of the ^{241}Am results. To ascertain signal detectability for these measurements, we followed the method of limits of detectability as described by Knoll in the book *Radiation Detection and Measurement* (Chapter

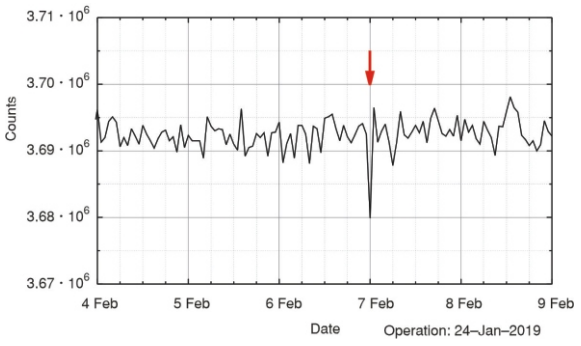

Figure 4. The ^{241}Am gamma radiation counts per hour, results in/from thirteen days after cyclotron operations. The arrow indicates the ^{241}Am dip due to neutrinos emitted from the cyclotrons

3, Section VI) [30]. Knoll's description explains how to detect real activity above the background. However, in our case, we need to inspect the decrease in the count rate (signal) below the mean count rate. Following Knoll's method, we implemented the 'limits-of-detectability' approach: *There is a 95 % probability that a random sample will lie below the mean plus 1.645* [30]. Dips critical level (LC) was calculated using the neighboring counts average. Subsequently, dip counts were compared to the LC. Once the presented dip counts were below the LC value, it was clear that a reliable signal was detected and thus could be accepted as a valid result. Statistical significance calculations were performed and are shown in eqs. (18)-(23) in the Supplementary information section.

According to the calculations, if a change is greater than |"0.11"| %, the signal exceeds the critical level, and it is a reliable result. Repetition and uniformity are evident in all nine dips the percentage of decrease in the reading is higher than 0.11 %. Therefore, all nine dips are considered statistically significant. Additionally, the range of numbers of from the average counts for all 9 dips was calculated, Supplementary information eq. (23), as shown in tab. 2.

The ^{222}Rn system

Thirteen dips in ^{222}Rn count rates were observed, responding to dual cyclotron operations. The 100 kBq ^{222}Rn activity (and its progeny) was continuously produced by a ^{226}Ra-226 source placed in a freezer at – 40 Celsius degrees. The data was collected from the NaI(Tl) detector at 15 minute intervals. The dip results are summarized in tab. 4 in the Supplementary information. Figure 5 shows two examples of changes in ^{222}Rn count rates.

Statistical significance calculations were performed using the *limits-of-detectability* method, as described in the Supplementary information (eqs. 18-23, using the data obtained from ^{222}Rn results). A percentage of LC (%LC) was calculated and found to be 0.41 %.

Accordingly, when the change in the count rate is greater than |"0.41" | %, the dip is considered valid.

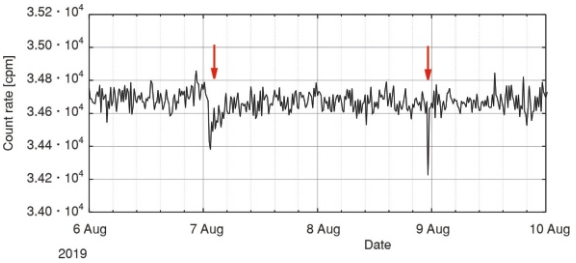

Figure 5. The ^{222}Rn count rate changes resulting from the operation of two different cyclotrons; the two arrows indicate the dips in ^{222}Rn due to neutrinos emitted from the cyclotrons; the left arrow denotes a dip after 11.5 hours, and the right arrow denotes a dip 19.25 hours after operation time

Repetition and uniformity are evident in all registered dips the percentage of decrease in readings is higher than 0.41 %. Therefore, all dips presented in tab. 4 are considered statistically significant. The range number of of the dips from the average counts for ^{222}Rn results is summarized in tab. 2.

Thorium system

Six operations of the cyclotrons caused six decreases in the gamma count rate of the system. Thorium, in the form of $Th(NO_3)_4$, is a naturally occurring radioactive material (with its progeny) with about 500 kBq. Figure 6 shows an example of a decrease in counts due to cyclotron operation. Simultaneously, we performed similar measurements using a similar thorium source and a similar detector at a laboratory located more than 50 km away from a cyclotron (henceforth called the control lab). The measurements yielded by the two systems, one near a cyclotron and one far from it, are presented in the Supplementary information, fig. 8, and indicate that the dip occurred only in the system near the cyclotron. This comparison confirms that the detected dip originated solely from the cyclotron operation. Thorium results are presented in tab. 5 in the Supplementary information.

Statistical calculations concerning the thorium results were performed using the same equations applied to ^{241}Am (eqs. (18)-(23) in the Supplementary information). The percentage of LC (%LC) was found to be 0.14 %. Repetition and uniformity are evident in all registered dips the percentage of decrease in the reading is higher than 0.14 %. Therefore, all dips presented in tab. 5 are considered statistically significant. The range of the number of from the average counts for the Thorium dips is summarized in tab. 2.

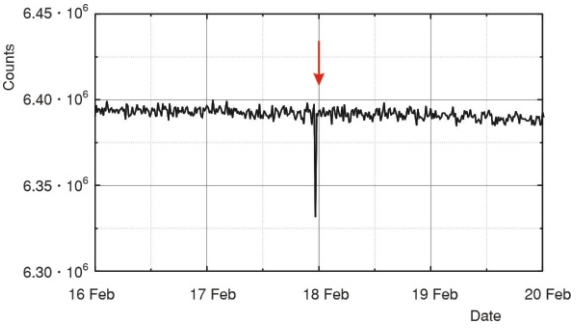

Figure 6. Counts per 15 minutes measurements for thorium. A decrease in count rate occurred on 17 February 2020 (marked with arrow) due to changes in the neutrino flux emitted by the operation of cyclotrons on 11 February

The ^{57}Co system

Twelve decreases in ^{57}Co counts were detected following twelve operations of the cyclotrons, as listed in tab. 6 in the Supplementary information. Figure 7 presents one example of the ^{57}Co response to neutrinos emitted from cyclotron operation.

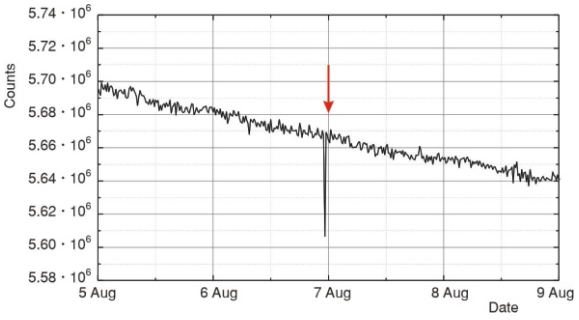

Figure 7. A dip, marked with arrow, in the measured counts (per 15 minutes) of ^{57}Co caused by cyclotron operation on 29 July 2020

The measurements for ^{57}Co counts demonstrate a downward trend since the source decays relatively rapidly due to its half-life of 272 days. The calculation of standard deviation is based on averaging 200 data points (~2 days measured points), where the trend is less significant. Data points were averaged on both sides around the count decrease that occurred in 06-Aug-2020, as shown in fig. 7, the average counts of both sides are required to reduce regular fluctuations from readings [30]. Calculations for ^{57}Co obtained a %*LC* of 0.32 % and % of 0.137 %. Therefore, we obtained decreases ranging from 6.7 σ to 11.6 σ from the trend line. Repetition and uniformity are evident in all twelve dips-the percentage of decrease in readings is higher than 0.32 %. Hence, all twelve dips are considered statistically significant.

Table 2 summarizes all the statistical considerations for the results of each radiation system.

Table 2. Range of the dips counts change measured by each radiation system, and the overall results' statistical significance

Source	Change [%]		Range of dip distance from mean
^{241}Am	(–0.21)-(–0.38)	0.049	4.3-7.7
^{222}Rn	(–0.48)-(–1.3)	0.176	2.7-7.4
Thorium	(–0.97)-(–1.07)	0.060	16.2-17.8
^{57}Co	(–0.95)-(–1.63)	0.137	6.7-11.6

DISCUSSION

The possible argument that the measured count decreases are fluctuations resulting from the detector's instability was ruled out by conducting an identical experiment using a 3" 3" NaI(Tl) detector connected to a multi-channel analyzer facing a source (*e. g*., thorium). The peaks of the energy lines obtained were stable, no spectral shifts were observed, and the measured peaks matched the characteristic spectrum of the radioactive nucleus [41].

The ^{222}Rn (and progeny) and thorium (and progeny) were used in our measurement systems; both these sources have decay chains that consist of alpha and beta(–) emissions. The system of these experiments detects the gamma radiation from the overall decay chain emission. Therefore, at this stage, we could not distinguish which emission was suppressed. However, since ^{234}Th/^{230}Th decay toward ^{222}Rn, which was measured with a difference delay compared to the indicated decrease measured in the thorium system, we can assume that the measured dips in the thorium system are from the gamma radiation of the ^{232}Th chain.

The ^{241}Am decays to ^{237}Np, which is a long half-life isotope. Therefore, in the ^{241}Am spectrum (above 40 keV), our system can only detect the 60 keV of ^{241}Am. Thus, our finding corresponds only to the ^{241}Am disintegration.

The ^{57}Co decays to stable ^{57}Fe, and our system can only detect its gamma radiation emission. Therefore, our results indicated only the ^{57}Co decay decrease.

The results for the four radioisotopes indicate that gamma radiation count rates were suppressed. In two radioisotopes, the decrease is direct via the prime decay, while in the case of the two other radioisotopes, the decrease can be related to other decays along the decay chain, in alpha or betta emissions.

From the range of for each source, we found that ^{57}Co and thorium systems exhibited a much more significant response to the change in cyclotron neutrino flux.

In all the results, the calculated for the count decreases was higher than the fluctuation range (above the calculated Lc (26), as presented in tab. 2); therefore, the observed decreases can be considered reliable results.

CONCLUSIONS

Several studies of radioactive nuclei have indicated that solar flares modify the radioactive decay constant. Yet, there was doubt regarding what factor in the solar flares affected the change in radioactive decay constant.

Proton cyclotrons produce several types of radionuclides that emit neutrinos along with their decay, with a relatively high rate during a short period, around one hour or less. Therefore, the cyclotron provides a controlled and predicted neutrino source. Since the measurement system was placed close to the cyclotrons, only electron-neutrinos certainly reached the system.

In this study, repetitions were conducted for each measurement system to assure the validity of the results, and the attribution of the observed effect. Based on this study, we conclude that decreases in the decay rates for all the radioactive sources measured are due to an increase in the neutrino flux that penetrated the nucleus.

It is well known that neutrino detection is usually a very intricate task involving large stable matter detectors. However, in this study, the neutrino interacted with an unstable nucleus that could reveal different types of physical detection processes. The radioactive nucleus differs from a stable nucleus in that it has a nu-

cleon occupying the occupied in higher energy levels. We assume that in the case of a radioactive nucleus, a neutrino could be captured in the nucleus shell structure, and this may explain the count rate alteration. This phenomenon indicates that further modeling of nuclear processes should be considered in the case of unstable nuclei in which a neutrino may be included in the internal nucleon structure.

The obtained count decreases could be explained by magnetic neutrino interactions with the nucleus spin, which in turn influence the momentum selection rules of the gamma emission multipolarity, *slowing down* the radioactive nucleus decay rate and the emission of gamma radiation.

This study presents findings regarding the initial effect of the neutrino on radioactive nuclei. Therefore, the theoretical aspects and mechanism of the process have yet to be investigated.

SUPPLEMENTARY INFORMATION

To ascertain signal detectability for the measurements reported in the results and discussion section, we implemented the method of limits-of-detectability as described in the book *Radiation Detection and Measurement* (chapter 3 section VI) [30]. Statistical calculations were done on 200 signals measured before or after the occurrence of a dip. First, the average of the signal was calculated (Mean) and the standard deviation . Then, the implementation of Knoll's limits-of-detectability method was used to evaluate whether the dip was *real*. An example of statistical calculations for the dip in ^{241}Am results from 06-Feb-2019 (fig. 4), where the counts were 3679900, the mean value is 3692067.74, and σ is 1795.51, is shown below

$$LC \quad 2.326\ \sigma \quad 2.326\ 1795.51 \quad 4176.359 \tag{18}$$

$$\text{Mean} \quad LC \quad 3692067.74 \quad 4176.359 \quad 3687891.38 \tag{19}$$

$$\%LC \quad 1 \quad \frac{\text{Mean} \quad LC}{\text{Mean}} \quad 100\,\% \quad 0.11\,\% \tag{20}$$

According to this calculation, if a change is greater than |0.11 | %, the signal exceeds the critical level, and it is a reliable result.

Additionally, the distance of a dip from the average counts, in severa σ, was calculated by dividing the percentage of the decrease of the count rate (% dip) by the percentage of σ (% σ).

$$\%\sigma \quad \frac{\sigma}{\text{Mean}} \quad \frac{1795.5}{3692067.74}\ 100\,\% \quad 0.049\,\% \tag{21}$$

$$\%\text{dip} \quad \frac{\text{dip}}{\text{Mean}} \quad \frac{3679900}{3692067.74}\ 100\,\% \quad 0.38\,\% \tag{22}$$

$$\text{Number of}\ \sigma = \frac{\%\text{dip}}{\%\sigma} \quad \frac{0.38\,\%}{0.049\,\%} \quad 7.7\,\sigma \tag{23}$$

From these calculations, a signal of 7.7 times was obtained. The same method was used to calculate the number of s for all 9 dips measured in the Am system, and the results ranged between: 4.3 and 7.7. This calculation method was performed on all four measurement systems, and the ranges were summarized, tabs. 3-6.

To confirm our premise, that neutrino flux affects radioactive decay, simultaneous measurements of a similar thorium source were conducted in the separate control laboratory, located more than 50 kilometers from any cyclotron accelerator. Figure 8 demonstrates the differences in the measurements between the two laboratories. The neutrino flux emitted from the cyclotron is the cause of the dip in the measurements of the radioactive thorium source.

Table 3. Dual cyclotron operations summary and the corresponding ^{241}Am system responses

Date of cyclotron operation	Date of sharp dip	Delay [d]	Count decrease [%]
24-Jan-2019	06-Feb-2019	13	–0.38
06- Feb-2019	19- Feb-2019	13	–0.27
19 Feb-2019	04-Mar-2019	13	–0.24
04-Mar-2019	17-Mar-2019	13	–0.28
18-Mar-2019	29-Mar-2019	11	–0.29
28-Mar-2019	12-Apr-2019	12	–0.30
15-Apr-2019	26-Apr-2019	11	–0.21
29-Apr-2019	12-May-2019	13	0.22
14-May-2019	28-May-2019	15	–0.26

Table 4. Summary of all cyclotron operations and ^{222}Rn system responses

Cyclotron operation time	Sharp dip time	Delay [h]	Count decrease [%]
01-Aug-2019 08:20	01-Aug-2019 13:00	05:30	–0.53
06-Aug-2019 14:00	07-Aug-2019 01:30	11:30	–0.77
08-Aug-2019 04:00	08-Aug-2019 23:15	19:15	–1.30
25-Sept-2019 07:15	25-Sept-2019 23:15	16:00	–1.15
18-Nov-2019 10:00	18-Nov-2019 23:15	13:15	–1.13
19-Nov-2019 08:00	19-Nov-2019 20:00	12:00	–0.48
21-Nov-2019 02:00	21-Nov-2019 13:30	11:30	–0.71
21-Nov-2019 11:30	21-Nov-2019 23:45	12:15	–0.62
26-Nov-2019 16:45	27-Nov-2019 07:15	14:30	–0.74
16-Dec-2019 10:00	16-Dec-2019 22:15	12:15	–0.70
24-Dec-2019 14:30	25-Dec-2019 23:15	8:45	–1.03
26-Jan-2020 11:00	26-Jan-2020 23:15	12:15	–1.08

Table 5. Summary of cyclotron operations and resulting thorium system responses

Date of cyclotron operation	Date of sharp dip	Delay [d]	Count decrease [%]
11-Feb-2020	17-Feb-2020	7	–0.97
23-Feb-2020	02-Mar-2020	9	–1.06
10-Mar-2020	19-Mar-2020	10	–0.98
02-Apr-2020	14-Apr-2020	13	–1.07
22-Apr-2020	03-May-2020	12	–1.05
14-May-2020	23-May-2020	10	–0.99

Table 6. Summary of all ^{57}Co system responses to cyclotron operations

Date of cyclotron operation	Date of sharp dip	Delay [d]	Count decrease [%]
07-Jul-2020	12-Jul-2020	5	–1.06
29-Jul-2020	06-Aug-2020	9	–1.07
25-Aug-2020	31-Aug-2020	7	–1.02
24-Sept-2020	27-Sep-2020	4	–0.95
13-Oct-2020	20-Oct-2020	8	–0.98
08-Dec-2020	14-Dec-2020	7	–1.12
21-Dec-2020	27-Dec-2020	7	–1.10
31-Dec-2020	08-Jan-2021	9	–1.20
14-Jan-2021	20-Jan-2021	6	–1.06
19-Jan-2021	25-Jan-2021	6	–1.63
01-Feb-2021	06-Feb-2021	5	–1.07
09-Feb-2021	18-Feb-2021	9	–0.96

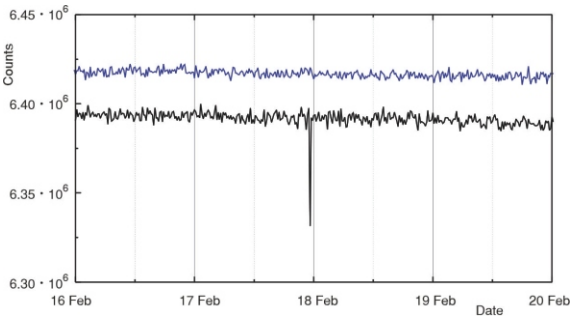

Figure 8. Comparison of thorium measurements conducted in two separate systems, one located near a cyclotron (the bottom graph) and the other located more than 50 kilometers away from any cyclotrons (he above graph)

ACKNOWLEDGMENT

We thank Eyal Mishani and Amiram Azarzar from S. R. Y. Medical Services, Jerusalem, Israel for their assistance in the cyclotron operations. We thank Dr. Rebecca Wolpe for the language editing of this manuscript.

AUTHORS' CONTRIBUTIONS

Conceptualization: I. Orion; formal analysis: J. Walg; investigation: I. Orion, J. Feldman, J. Walg; methodology: J. Feldman; supervision: I. Orion; writing-original draft: J. Walg; writing-review and editing: I. Orion.

ORCIID NO

Jonathan Walg https://orcid.org/0000-0002-5185-9283
Jon Feldman https://orcid.org/0000-0001-9485-3925
Itzhak Orion https://orcid.org/0000-0001-5067-2102

REFERENCES

[1] Jenkins, J. H., Fischbach, E., Perturbation of Nuclear Decay Rates During the Solar Flare of 2006 December 13, *Astroparticle Physics, 31* (2009), 6, pp. 407-411
[2] Pomme, S., Pelczar, K., Neutrino-Induced Decay: A Critical Review of the Arguments, *Space Sci Rev., 218* (2022), 64, https://doi.org/10.1007/s11214-022-00932-0
[3] Pomme, S., *et al*., On the Interpretation of Annual Oscillations in ^{32}Si and ^{36}Cl Decay Rate Measurements, *Sci Rep., 11* (2021), https://doi.org/10.1038/s41598-021-95600-8
[4] Pomme, S., Pelczar, K., Kajan, I., Air Humidity and Annual Oscillations in ^{90}Sr/^{90}Y and ^{60}Co Decay Rate Measurements, *Sci Rep., 12* (2022), https://doi.org/10.1038/s41598-022-13841-7
[5] Pomme, S., Pelczar, K., On the Recent Claim of Correlation Between Radioactive Decay Rates and Space Weather, *Eur. Phys. J., C 80* (2020), https://doi.org/10.1140/epjc/s10052-020-08667-4
[6] Lapp, R. E., Andrews, H. L., Nuclear Radiation Physics. Second Ed. pp. 72 (1954) (Prentice-Hall Inc., Upper Saddle, River, N. J. USA)
[7] Alburger, D. E., Harbottle, G., Norton, E. F., Half-Life of ^{32}Si, *Earth and Planetary Science Letters, 78* (1986), 2-3, pp. 168-176
[8] Holstein, B. R., Weak Interactions in Nuclei, Princeton University Press (2017), https://doi.org/10.1515/9781400887040
[9] Reines, F., Cowanjun, C., The Neutrino, *Nature 178* (1956), pp. 446-449, https://doi.org/10.1038/178446a0
[10] Capozzi, F., *et al*., Masses and Mixings: Status of Known and Unknown 3v Parameters, *Nuclear Physics., B 908* (2016), July, pp. 218-234
[11] Battye, R. A., Moss, A., Evidence for Massive Neutrinos from Cosmic Microwave Background and Lensing Observations, *Phys. Rev. Lett., 112* (2014), https://link.aps.org/doi/10.1103/PhysRevLett.112.051303
[12] Davis, R., Harmer, D. S., Hoffman, K. C., Search for Neutrinos from the Sun, *Phys. Rev. Lett., 20* (1968), pp. 1205-1209 https://link.aps.org/doi/10.1103/PhysRevLett.20.1205
[13] Hampel, W., Particle Physics: How to Detect Solar Neutrinos, *Nature, 318* (1985), pp. 312-313 https://doi.org/10.1038/318312a0
[14] Davis, R., A Review of Measurements of the Solar Neutrino Flux and Their Variation, *Nuclear Physics B - Proceedings Supplements, 48* (1996), pp. 284-298, https://doi.org/10.1016/0920-5632(96)00263-0
[15] Essig, R., Sholapurkar, M., Yu, T. T., Solar Neutrinos as a Signal and Background in Direct-Detection Experiments Searching for sub-GeV Dark Matter with Electron Recoils, *Phys. Rev., D 97* (2018) https://link.aps.org/doi/10.1103/PhysRevD.97.095029

[16] ***, The Borexino Collaboration, Experimental Evidence of Neutrinos Produced in the CNO Fusion Cycle in the Sun, *Nature, 587* (2020), pp. 577-582 https://doi.org/10.1038/s41586-020-2934-0
[17] Kodama, K., *et al*., Final Tau-Neutrino Results from the DONuTexperiment, *Physical Review, D 78* (2008), https://link.aps.org/doi/10.1103/PhysRevD.78.052002
[18] Aartsen, M. G., *et al*., The IceCube Collaboratio, Measurement of the Multi-TeV Neutrino Interaction Cross-Section with IceCube Using Earth Absorption, *Nature, 551* (2017), pp. 596-600 https://doi.org/10.1038/nature24459
[19] Goncharov, M., *et al*., Precise Measurement of Dimuon Production Cross-Sections in ν Fe and $\bar{\nu}_{\mu}$ Fe Deep Inelastic Scattering at the Tevatron, *Phys. Rev., D 64* (2001) https://link.aps.org/doi/10.1103/PhysRevD.64.112006
[20] Stein, R., *et al.*, A Tidal Disruption Event Coincident with a High-Energy Neutrino, *Nat Astron, 5* (2021), pp. 510-518 https://doi.org/10.1038/s41550-020-01295-8
[21] Abreu, H., *et al*., First Neutrino Interaction Candidates at the LHC., *Phys. Rev., D 104* (2021) https://link.aps.org/doi/10.1103/PhysRevD.104.L091101
[22] Halzen, F., Kheirandish, A., Black Holes Associated with Cosmic Neutrino Flares, *Nat. Phys., 16* (2020), pp. 498-50 https://doi.org/10.1038/s41567-020-0864-2
[23] Aprile, E., *et al*., Observation of Two-Neutrino Double Electron Capture in ^{124}Xe with XENON1T, *Nature 568* (2019), pp. 532-535 https://doi.org/10.1038/s41586-019-1124-4
[24] Walg, J., Rodnianski, A., Orion, I., Evidence of Neutrino Flux effect on Alpha Emission Radioactive Half-Life, *Proceedings*, Series ATINER's, PHY2019-0137 Athens, 2019
[25] Walg, J., Peleg, Y., Rodnianski, A., Hazenshprung, N., Orion, I., The Effect of Solar Flares on ^{54}Mn and ^{57}Co Radioactive Decay Constants Performance, *Nucl Technol Radiat, 36* (2021), 3, pp. 219-223
[26] Walg, J., Rodnianski, A., Orion, I., Solar Flare Detection Method Using Rn-222 Radioactive Source, *GSC Advanced Research and Reviews, 05* (2020), pp. 159-166 https://doi.org/10.30574/gscarr.2020.5.2.0087
[27] Peleg, Y., Orion, I., The Impact of Strong Solar Flares on Thorium Beta Radiation Count-Rate, *Nucl Technol Radiat, 38* (2023), 2, pp. 102-107
[28] Davis, R. Jr., Evans, J. C., Cleveland, B. T., The Solar Neutrino Problem, *AIP Conference Proceedings, 52* (1979), pp. 17-27, https://doi.org/10.1063/1.31802
[29] Davis, R. Jr., Evans, J. C., Cleveland, B. T., E. C. Fowler (Ed.), *Proceeding*, Neutrino Physics, Purdue U. P. West Lafayette, 1978
[30] Knoll, G. F., Radiation Detection and Measurement, 3rd ed., *John Wiley and Sons* (2000), Ch. 3 & 8 &9
[31] Birks, J. B., The Theory and Practice of Scintillation Counting, Pergamon Press Ltd (1964) https://doi.org/10.1016/B978-0-08-010472-0.50004-5
[32] Lawrence, E. O., Livingston, M. S., The Production of High Speed Light Ions Without the Use of High Voltages, *Phys. Rev., 40* (1932), pp. 19-35 https://link.aps.org/doi/10.1103/PhysRev.40.19
[33] Chadwick, J., The Cyclotron and its Applications*, *Nature, 142* (1938), pp. 630-634 https://doi.org/10.1038/142630a0
[34] Mann, W., Recent Developments in Cyclotron Technique, *Nature, 143* (1939), pp. 583-58 https://doi.org/10.1038/143583a0
[35] Michaelis, E., Cyclotrons of All Shapes and Sizes, *Nature, 257* (1975), pp. 270-271 https://doi.org/10.1038/257270a0
[36] Alfassi, Z., Zlatin, T., German, U., Simultaneous Measurement of Gamma-Rays and Neutron Fluences Using a HPGE Detector, *J Radioanal Nucl Chem, 268* (2006), pp. 237-241 https://doi.org/10.1007/s10967-006-0186-6
[37] Walg, J., *et al*., Cyclotron-Produced Neutrons Measurements Using Chlorine Activation, *Nuclear Inst. and Methods in Physics Research, B 503* (2021), pp. 1-5. https://doi.org/10.1016/j.nimb.2021.07.001
[38] Stocklin, G., Pike, V. W., Radiopharmaceuticals for Positron Emission Tomography Methodological Aspects, Kluwer Academic Publishers, Boston, Mass, USA, 1993 web site http://www.nucleide.org/
[39] Rostampour, M., *et al*., Experimental Study and simulation of ^{63}Zn Production Via Proton Induce Reaction, *Applied Radiation and Isotopes, 136* (2018), pp. 32-36 https://doi.org/10.1016/j.apradiso.2018.02.005
[40] Szelecsenyi, F., et al., Evaluated Cross-Section and Thick Target Yield Data Bases of Zn+p Processes for Practical Applications, *Applied Radiation and Isotopes, 49* (1998), pp. 1005-1032 https://doi.org/10.1016/S0969-8043(97)10103-8
[41] Orion, I., Changes in the Gamma Spectra of Radioactive Materials Affected by Altering Neutrino Flux, *EasyChair Preprint no. 8767* (2022), https://easychair.org/publications/preprint/Q4RK

Received on December 21, 2023
Accepted on June 10, 2024

Џонатан ВАЛГ, Џон ФЕЛДМАН, Јицак ОРАЈОН

ПРОМЕНЕ БРЗИНЕ РАСПАДА У РАДИОАКТИВНОЈ ГАМА ЕМИСИЈИ ПОД УТИЦАЈЕМ ПРОТОНСКОГ 18 MeV ЦИКЛОТРОНА

Претходни напори да се истраже промене у константама распада радиоактивних нуклида открили су да сунчеве бакље могу привремено да промене брзине радиоактивног распада. Стога је увиђање да ли спољни фактори утичу на брзине радиоактивног распада од виталног значаја за разумевање нуклеарних процеса. Ова студија настојала је да истражи ефекат неутрина на радиоактивна језгра конструисањем система за детекцију гама зрачења који користи радиоактивни извор испред система емисије неутрина. Одговарајући на операције циклотрона, сваки од четири детекциона система регистровао је да се брзина одброја гама смањује. Резултати ове студије потврђују да је пораст флукса неутрина утицао на брзине распада испитиваних радиоактивних нуклида. Овде пружамо значајне доказе да неутрини утичу на процес радиоактивног распада. Детекција неутрина је изазовна због мале апсорпције у стабилном језгру. Међутим, студија је открила већу вероватноћу интеракције радионуклида са неутрином.

Кључне речи: циклотрон, радиоактивност, неутрино, гама зрачење